University of Thi-Qar Journal of Science (UTJsci)
E-ISSN: 2709-0256, P-ISSN: 1991-8690, Vol. 11, No. 2, Dec,2024

# DFT study of Mn-doped $CeO_2$: The structural and electronic properties

Aqeel Mohsin Ali*[1a] and Nooraldeen A. Toama[2b]

[1]*Polymer Research Center, University of Basrah, Basrah, Iraq.*
[2]*Almaaqal University, Basrah, Iraq.*

[b]E-mail: nooraldeenaljabiri@yahoo.com
[a*]Corresponding author: aqeel.mohsin@uobasrah.edu.iq

Received:2024-05-10, Revised: 2024-08-02, Accepted:2024-08-30, Published:2024-12-31

***Abstract*—The structural and electronic characteristics of manganese doped cerium oxide are investigated by means of the density functional theory with Habbard parameter approach. Experimental evidence and other theoretical findings corroborate the computed electronic characteristics, bulk modulus, cell volume, and equilibrium lattice parameter for ceria. By replacing the Ce atom with Mn, the bond length, bulk modulus, cell volume, and lattice parameter are all reduced. In the meantime, we see a narrowing of the band-gap. Interestingly, it is seen that the strength of the oxygen occupied states to cerium empty states transition and the covalent nature of the cerium oxygen bond are both reduced when manganese is doped into ceria. The heavy manganese doped ceria system may be used for applications involving the spin dependent current and light absorption, since it exhibits steeper absorption peaks spanning from 3.0 to 3.44 eV of spin down and spin upper, respectively.**

***Keywords*—ceria, manganese doping, Hubbard parameter, electronic properties.**

## I. INTRODUCTION

This Ceria ($CeO_2$) has several uses in current catalytic technology, including three-way catalysts (TWCs), solid oxide fuel cells (SOFCs), and high oxygen storage capacity (OSCs) [1,2]. Various technological applications may be attributed to $CeO_2$'s oxygen vacancy creation and transit capabilities. In addition to its long history of use as an oxygen storage material, cerium oxide ($CeO_2$) has recently attracted attention as a material with optical component and laser hosting potential. Optical coatings, whether single or multilayered, have long made use of $CeO_2$ as a film material due to its high refractive index. It can effectively absorb ultraviolet radiation and is also used to safeguard light-sensitive items by adding it to glass (2−4% $CeO_2$). There have been reports suggesting cubic $CeO_2$ as a possible alternative to rutile $SnO_2$ [3] and $TiO_2$[4]. According to Veszelei et al.,[4] $CeO_2$ outperformed $TiO_2$ under the influence of light of $\lambda < 400$ nm due to its significant absorption. In contrast to $TiO_2$-rutile, Miyauchi et al [5] .hypothesized that cerium dioxide's considerably smaller photocatalytic behavior reduced the deterioration of the compound containing ultraviolet absorber species by limiting the generation of reactive oxygen species.

According to Goubin et al. [6], ceria has a refractive index of 2.35, a strong UV absorption rate, and a band gap of 3.2 eV. The fact that transition metals are characterized by a short ionic radius and a strong valence is intriguing. The electrical structure of transition metals is comparable to that of noble metals. To boost the performance of mental oxide, the current catalytic industry commonly uses transition metals, which are excellent modified elements. To illustrate the significant impact on electrical and magnetic characteristics, Park et. al [7]. investigated the effects of atomically-substitution doping of 3d transition metals in titanium dioxide. They determined that reducing the band gap by doping $TiO_2$ with Fe (or Co, Ni) was the result; ground states of Ni-doped $TiO_2$ are paramagnetic, whereas ground states of Co-doped $TiO_2$ are antiferromagnetic. In contrast, systems that include iron do have ground states with magnetic properties that include orbital components of magnetism. The structural and optical characteristics of ZnO were studied by Anghel et al.[8], who evaluated the impact of doping by various transition metal ions on these properties. They discovered that doping with chromium, manganese, iron, cobalt, or nickel had a substantial influence on both the electrical and optical aspects of the material. According to the calculations done by Kim and Bishop et. al [9]. on ceria that has been doped with transition metal praseodymium (Pr) and its optical absorption spectrum, the appearance of the Pr doping electronic states inside the band gap of $CeO_2$ caused a wide response of light in the visible spectrum from 2.0-3.3 eV, giving the material a reddish-orange hue. The optoelectronic characteristics of pure and metal doped $CeO_2$ have piqued the interest of scientists, and there are tests demonstrating that the material's properties are modified or enhanced when transition metals like iron, cobalt, or nickel are doped into the material. As an example, in an experiment, Li and Wang et. al [10]. utilized the co-precipitation method to create a variety of $Ce_{1-x}Fe_xO_2$ (x=0, 0.2, 0.4, 0.6, 0.8, and 1) complex oxide catalysts. Among these, they discovered that $Ce_{1-x}Fe_xO_2$ exhibited a high capacity for oxygen storage, excellent redox firmness, and intensive interaction between both cerium and iron species. Through experimental investigation of the optical characteristics of cobalt-doped


https://doi.org/10.32792/utq/utjsci/v11i2.1252

ceria, Ranjith et al [11]. discovered that the introduction of cobalt ions into Ce shifted the optical response peak across longer wavelengths, resulting in a shift in the visible spectrum. An experiment conducted by Kumar et al [12]. on Ni-doped $CeO_2$ nanoparticles revealed a drop in the lattice parameters computed using Powder-X software, from 5.41 to 5.40Å, indicating an investigation into the structural and magnetic characteristics of these particles. There has been a dearth of theoretical investigation on the crystal and optoelectronic characteristics of $CeO_2$ doped with 3d-transition metals. D. Tian et al [13]. studied $CeO_2$ doped with transition metals (Fe, Co, or Ni) by using GGA+U approximation and characterized the structural and optoelectronic properties.

Doping manganese (Mn) with metal oxides improves the optical characteristics of its composites, which already have strong optical qualities. When doped with metal oxides, it exhibits desirable magnetic properties. The magnetic properties of Mn-doped materials are enhanced at low temperatures. It seems that the electrical and dielectric characteristics of materials doped with Mn are better. M. Sharma et al [14]. investigated the energy storage application of Mn-$CeO_2$, and they showed that the specific capacitance and capacitance retention has been increased. By applying first-principles calculations to the redox characteristics of M-doped $CeO_2$ (where M = Mn, Pr, Sn, and Zr), Tang et al [15]. discovered that structural distortion was the main source of the O-vacancy formation energy decrease for Zr-doped $CeO_2$, whereas electronic modification and structural distortion combined to cause the same decrease for Mn-, Pr-, and Sn-doped $CeO_2$. Prabaharan et al.[16] presents an in-depth review of the synthesizing and characterizing of Cerium oxide ($CeO_2$) nanoparticles, including structural, morphological, optical, and electrical studies, as well as those including Mn doping. They demonstrated that the absorption of both pure and Mn-doped particles took place in the ultraviolet spectrum. Pintos et al [17]. investigated the geometric and electronic properties of 12.5% Mn-doped $CeO_2$ using DFT+U periodic calculations. The results show that the Mn-dopant enhances the formation of structural O-defects, releases surface active oxygen atoms, and increases bulk anionic mobility. These findings provide light on Mn-doped $CeO_2$ performs so well in oxidation reactions.

Now is the moment to study these systems' structures and optical characteristics, since they may induce novel electronic structures that might lead to new applications. We conducted first-principles calculations to study the structural, and electronic properties of $CeO_2$ and transition metal manganese doped $CeO_2$ ($Ce_{1-x}Mn_xO_2$, where x is the concentration of doping) using the density functional theory (DFT) method within the generalized gradient approximation (GGA)[18]. This study is performed to shed light on the manganese doped $CeO_2$ electronic properties.

## II. Modelling Method

The cerium dioxide has a crystal structure of face-centered cubic, and the system can be described by space group Fm-3m (number 225 in the international tables). The Ce ions ($Ce^{+4}$) are arranged by 8-valent nearest-neighbor oxygen ions ($O^{-2}$) at one corner of the cube, and the O atoms are surrounded by four Ce atoms in tetrahedrally coordinated, as shown in Fig. 1(a). A 25% Mn concentration is achieved in the doped systems ($Ce_{0.75}Mn_{0.25}O_2$) by exchanging one Ce atom for one Mn atom in a 12-atom supercell. Because $CeO_2$ has a perfectly symmetrical structure and just one cation site, the site preference is irrelevant when replacing the Ce atom with Mn. The model of 1 × 1 × 1 unit cell with 12 atoms (4-Ce and 8-O atoms) was used as the basic model to explore the optical characteristics, band structure, and lattice parameter of $Ce_{1-x}Mn_xO_2$ (x=0, 0.25). Fig. 1(a, b) represents pure ceria and Mn doped ceria, respectively. In order to simulate a neutral impurity of Mn in $CeO_2$, we replaced the Ce atom with a Mn atom; the resultant unit cell are $Ce_{0.75}Mn_{0.25}O_2$.

The first-principles computations are carried out in the CASTEP software via the use of the GGA and ultrasoft pseudopotentials for atoms inspection. In particular, PBEsol, the Perdew-Burke-Ernzerhof functional for solids,[19] is implemented for geometric optimization. Manganese (4s and 3d electrons) are considered valence electrons here, along with cerium electronic states (5s, 5p, 5d, 4f, and 6s).

The generalized gradient approximation (GGA) calculations also make use of PBESOL. The plane-wave basis set fixed to 500 eV for cutoff energy. There is a convergence tolerance of $5 \times 10^{-6}$ eV for the energy charge, 0.01 eV/A⁰ for the maximum force, and 0.02 GPa for the stress. The Broyden, Fletcher, Goldfarb, Shanno (BFGS) approach is used to optimize the geometry of the beginning model in order to reach the total system energy reducing. The $Ce_{1-x}Mn_xO_2$ (x=0, 0.25), electronic structure computation all make use of the 4 × 4 × 4 Monkhorst-Pack grid to achieve the Brillouin zones integration. The formation energy is estimated according to El-achari et al. procedure [20].

## III. Results and Discussin

During the geometry optimization procedure, all internal coordinates as well as the lattice constants are loosened in order to get the stable structure of $Ce_{1-x}Mn_xO_2$. Fig. 2 showed the optimization procedure for lattice constant. Tables I include the computed lattice constants, formation energy, bond length and cerium ion charge. Based on the data in Table I, it is clear that the approach presented in Part 2 of the design and calculation procedure provides a satisfactory description of the cerium dioxide crystal. The equilibrium lattice parameter, formation energy, and bond length were determined to be 5.41 Å, 4.5 (eV), and 2.361 (Å), respectively. The experimental values of the lattice constant, bond length and charge are all in accord with these values, and they are also in excellent agreement with other computations. The length of lattice constant is found excellent prediction to the experimental value of $CeO_2$'s lattice constant $a_0$ = 5.41 (Å) when compared to Table I experimental data and values from other computations. According to the studies, the lattice constant $a_0$ for the $Ce_{1-x}Mn_xO_2$ structure (x=0.25) diminishes when Mn dopes ceria, as is evident from Table I. This is because $R_{Mn}^{+3}$=0.645 Å and $R_{Ce}^{+4}$=0.97 Å, which are the covalent radii of $Mn^{+3}$ and $Ce^{+4}$, respectively. Accession the Mn dopant heavy concentration resulted in a lowering of the lattice parameter. According to Table I, the structure of

$Ce_{1-x}Mn_xO_2$ (x=0.25) shows that cell volume and bond length are reduced after Mn doping of ceria. For Mn-doped $CeO_2$, this is likely due to the lattice distortion caused by the variations in covalent radii between $Mn^{+3}$ and $Ce^{+4}$. It was known that when Mn was doped into $CeO_2$, crystal defects formed around the dopants, and the resulting charge imbalance altered the materials' stoichiometry. After replacing the Ce atom with Mn, the bond lengths of Ce−O are reduced. The $Ce_{0.75}Mn_{0.25}O_2$ has a lesser maximum bond distance of 2.352 Å than the $CeO_2$ experimental values 2.366 Å as shown in Table I. This indicates that the ionic bond strength for cerium dioxide is greater than that of the $Ce_{1-x}Mn_xO_2$ system (with x=0.25). more lesser and higher than O-Ce-O angles. The ionic charge of $Ce^{+4}$ will reduced to $Ce^{+3}$ by accepting an extra electronic charge, and this reduction change the whole density of charge within the crystal. In this model, cerium exhibits a departure from its tight tetravalent state.

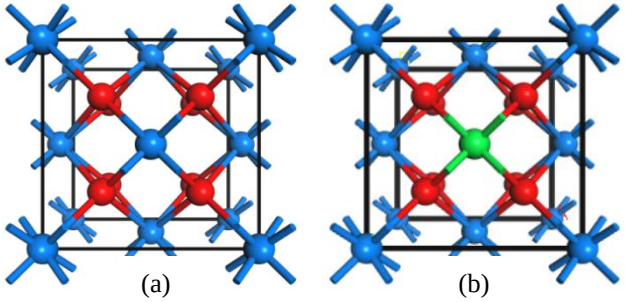


Fig. 1: Perspective projection of pure and doped ceria unit cell. a) $CeO_2$ and b) $Ce_{0.75}Mn_{0.25}O_2$, where Ce (●), O (●) and Mn (●).

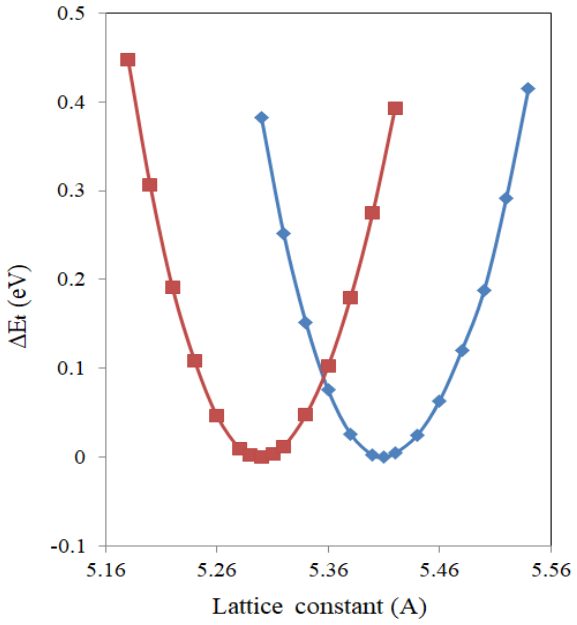


Fig. 2: Total energy difference ($\Delta E_t$) vs. lattice constant. (■) $CeO_2$ and (■) Mn-$CeO_2$.

TABLE I: lattice constant, formation energy, bond length and charge.

| Structure | $a_0$ (Å) | $E_f$ (eV) | Ce-O (Å) | Mn-O (Å) | Charge of Ce |
|---|---|---|---|---|---|
| $CeO_2$ | 5.410[a]<br>5.423[b]<br>5.480[c]<br>5.416[d]<br>5.470[e] | 4.5 [a] | 2.363[a],<br>2.35[b]<br>2.366[c] | -------- | +4[a] |
| Mn-$CeO_2$ | 5.300[a]<br>5.340[e] | 4.0 [a] | 2.352[a] | 2.33[a] | +3[a] |

[a]Present work.
[b]Reference [13], using GGA.
[c]Reference [21], using GGA.
[d]Reference [22], experimental.
[e]Reference [23], experimental.

It has been observed that the optical energy gap is often not accurate when using GGA calculations that rely on first principles calculations. This underestimation is attributed to inherent defects in the DFT calculation. In order to address the discrepancy, a technique known as the scissors operator (0.702 eV)" was implemented. This technique involves shifting the unoccupied conduction band relative to the valence band [25]. The electronic band structures of $Ce_{1-x}Mn_xO_2$ (x=0.0) have been plotted using a PBESOL level of theory in Fig. 3. It has been demonstrated that cerium dioxide has an indirect band gap value of 3.20 eV with an insulator characteristic. This finding aligns with previous reports and experimental data [26].

The energy band structure of Mn-$CeO_2$ has been plotted using a spin-polarized method in Fig. 4. It has been demonstrated that $Ce_{0.75}Mn_{0.25}O_2$ have a spin dependent band gap, and both of them are insulator with an indirect band gap value of 3.44 eV and 3.00 eV, for electron spin upper and electron spin down respectively, at the M-R points. When Ce is replaced by Mn in a doped system, there is a noticeable reduction for spin down electrons in the band gap ($E_g$). This indicates an augmentation in the conductivity of $Ce_{0.75}Mn_{0.25}O_2$. When Mn-atom is added to $CeO_2$, something interesting happens. The lattice structure gets distorted and there is a chance to reorganize the electron charge distribution, and to regulate the covalent character of Ce ions, this makes it easier for $Ce^{+4}$ to transform into $Ce^{+3}$. Doped $CeO_2$ has a symmetrical disposition of Ce with the same charge over all these cations. By increasing the amount of $Ce^{+3}$ states, localized energy states are formed that are in the vicinity to the conduction band. This leads to a decrease in the energy gap, as mentioned in [27]. Meantime, in the doped crystal, the conduction band widens (0.87 eV) compared to pure $CeO_2$ (0.54 eV), indicating an increase in metallic characteristics.

In the case of $Ce_{0.75}Mn_{0.25}O_2$, there is a noticeable impurity band within the band gap. Additionally, there is a clear expansion at the upper end of the valence band, resulting in a wider valence band width. The spin polarized electronic structure in Fig. 4 indicated separately electron spin upper and electron spin down optical response and electrical current. According to the spin dependent band gap of $Ce_{0.75}Mn_{0.25}O_2$, the wave length ($\lambda$) of optical response of electron spin down occur at lower energy and longer wave length ( $E_g$ = 3.00 eV, $\lambda$ = 413 nm ) than that

optical response of electron spin upper ( $E_g$ = 3.44 eV, λ = 360 nm). This a significant property of spin dependent electronic band structure present the 25% Mn doped $CeO_2$ may candidate for using in spintronic devices.

For a deeper understanding of the energy band structure, we have performed calculations to determine the partial density of states (PDOS) of $Ce_{1-x}Mn_xO_2$ system. These results have been plotted using the spin-polarized DFT method. In Fig. 5 and 6, the Fermi level is set to zero. It is primarily influenced by Ce-p, Ce-d, Ce-f, O-s, and O-p states. There are also minor contributions from Ce-s. The characteristics of O-2s states are localized between -19.0 and -11.2 eV below the Fermi level for pure $CeO_2$. These states are far below the energy of valance band which begin at 5.4 eV. Based on the information provided in Fig. 5, it is evident that the partial density of states indicate that $CeO_2$ is an insulator. This contradicts the previous band structure investigation. The valence band with the highest occupancy shows a noticeable mixing of O(2p) character, along with a small contribution from both the Ce(4f) state and Ce(4d) state. On the other hand, the narrow band located above the Fermi level is primarily attributed to the Ce(4f) states beside a tiny sharing of O(2p) electronic state which represented the conduction band. While this is going on, the DOS plot of our fluorite-type bulk structure reveals that the conduction band (CB) is separated from the VB by 3.2 eV, and there are several peaks in the gap (see Fig. 5). These unoccupied states that are located above the Fermi level are mostly created by O(2p), Ce(4f) and (4d) states, and they might be linked to the development of O(2p)-holes in the valence band.

It is possible that the abnormal physical properties of the material are a result of the significant correlation influences between the Mn(3d) state and the Ce(4f) state. In $Ce_{0.75}Mn_{0.25}O$, the VB constructed by O(2p) and a small participation of Mn(3d) electronic state, with a teeny involvement of Ce(4f) and Ce(4d) electronic states, see Fig. 6. While the conduction band is organized from Ce(4f) electronic state beside a tiny sharing of O(2p) electronic state, analogous that of pure $CeO_2$. The unoccupied states that are located above the Fermi level are mostly created by Ce(4f) with sharing of O(2p) states for both spin upper and down.

Meanwhile, the density of states (DOS) analysis of our manganese doped fluorite-type bulk structure reveals that the conduction band (CB) is located 3.0 (spin down) with red shift of O(2p) state, and 3.44 eV (spin upper) with blue shift of O(2p) state away from the valence band (VB), as shown in Fig. 6. Additionally, there is obvious unfilled O(2p) state present inside the conduction band in the case of spin down. In spin upper case, the unfilled O(2p) state cannot be seen clearly.

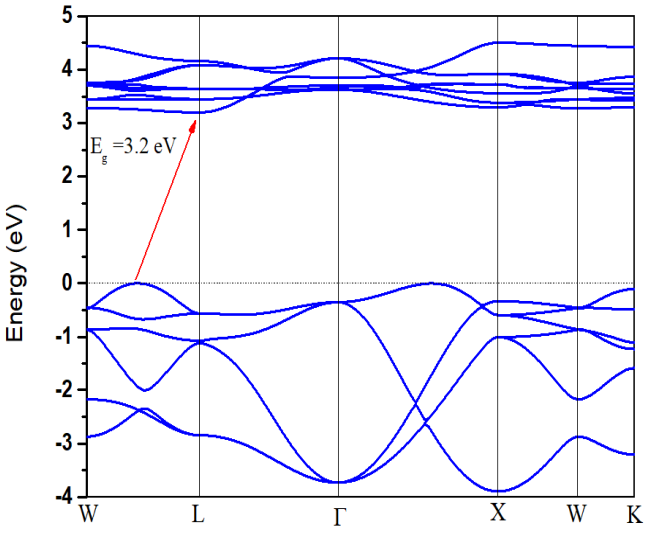


Fig 3: Electronic band structure of CeO2.

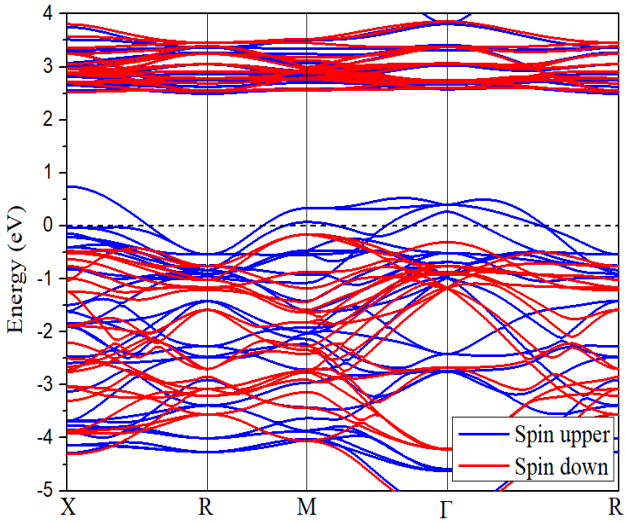


Fig. 4: Electronic band structure of Mn-doped CeO2.

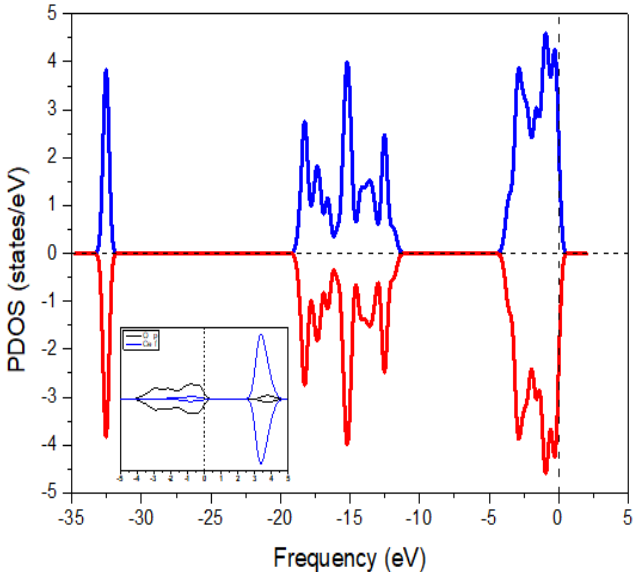


Fig. 5: Spin polarized PDOS of $CeO_2$.

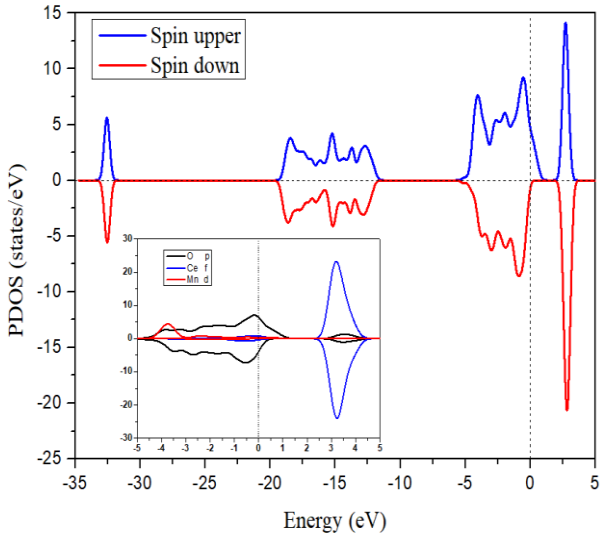


Fig. 6: Spin polarized PDOS of Mn-doped $CeO_2$.

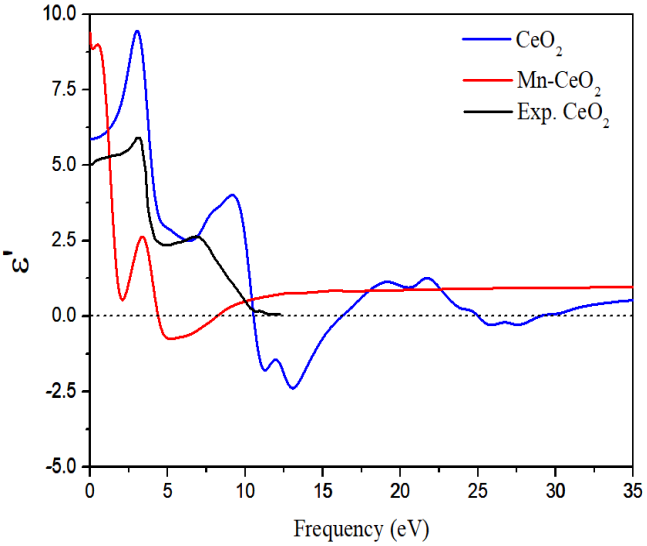


Fig. 7: Real part of dielectric function. Experimental data of $CeO_2$ from reference [28].

The imaginary component of the optical dielectric function $\varepsilon''$ has been obtained by averaging the interband transitions from filled to empty states in the density functional theory (DFT) findings. These transitions occur at energies far greater than those associated with phonons. Having knowledge of both the real and imaginary components of the dielectric tensor enables the calculation of many optical properties. This study presents and examines the reflectivity, absorption coefficient, refractive index n, and extinction coefficient k. Further elaboration on the optical computations was provided in another location.

The lower band gap of the doped system in comparison to pure $CeO_2$ results in higher absorption of visible light in the electromagnetic spectrum. Additionally, the lower refractive index suggests decreased reflection of visible light at the material-air interface. The introduction of Mn atoms into cerium dioxide ($CeO_2$) results in a shift of the absorption edge towards lower photon energies, leading to a red shift. This incorporation also decreases the refractive index, hence improving the ability to suppress light reflection, as shown in optical spectra. The computed optical properties (dielectric function and reflectivity) are qualitatively aligns closely with experimental findings [28].

Figure 2 shows the imaginary component of the dielectric function curves for photon energies ranging from 0 to 35 eV. Two distinct peaks, E1 and E2, are seen at energy levels of 3.2 eV and 10.5 eV, respectively, in the e2(w) spectrum. Additionally, a less prominent peak, E3, is observed at an energy level of 22 eV.

Upon comparing Figs. 2(b) and 2(c), we observed that in regions with high absorption, the reflectivity is correspondingly higher. If a certain kind of material has a significant ability to absorb light within a certain range, it will also have a high capacity to reflect light in the same region.

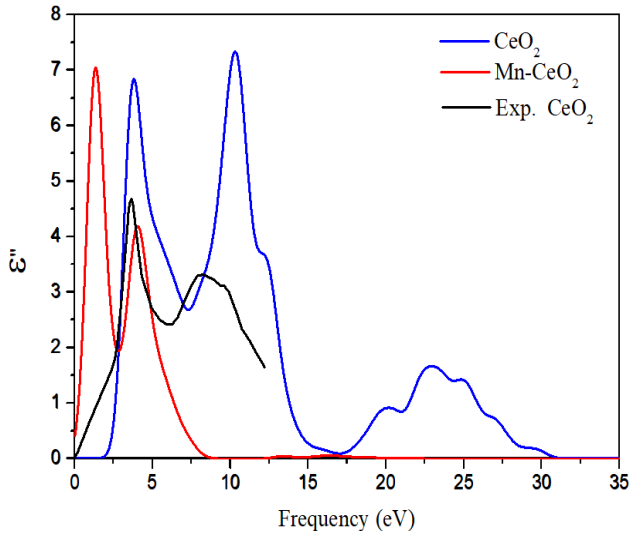


Fig. 8: Imagenary part of dielectric function. Experimental data of $CeO_2$ from reference [28].

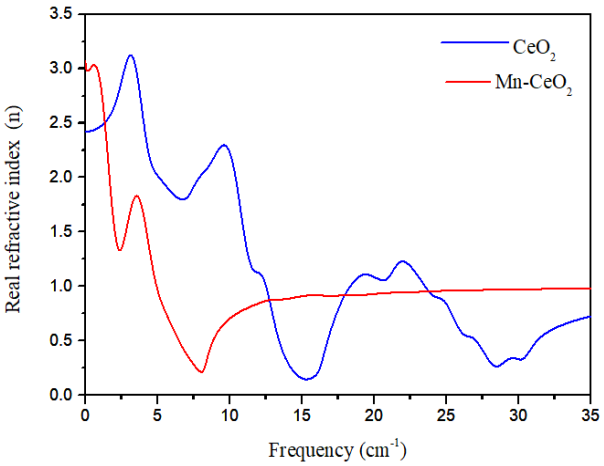


Fig. 9: Real part of refractive index.

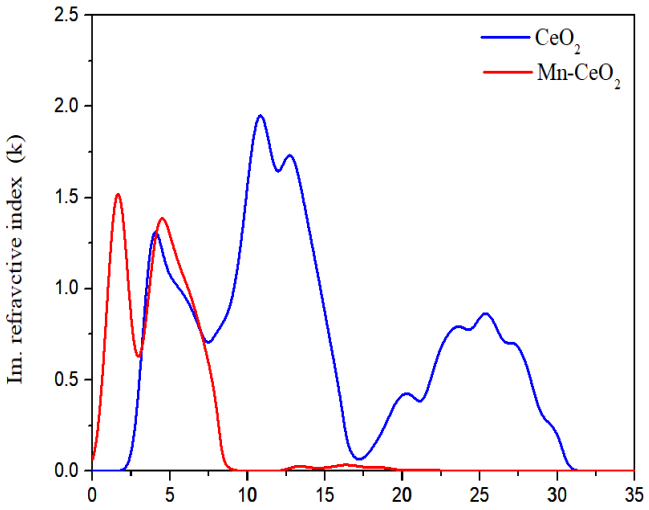


Fig. 10: Imagenary part of refractive index. Experimental data of $CeO_2$ from reference [28].

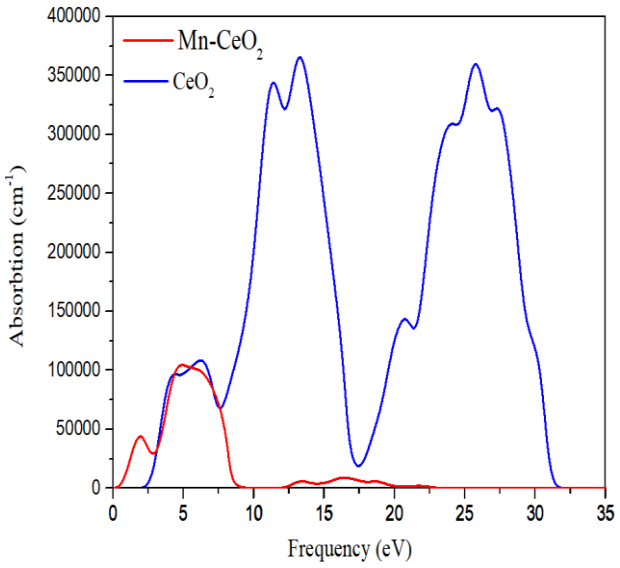


Fig. 11: Absorption coefficient. Experimental data of $CeO_2$ from reference [28].

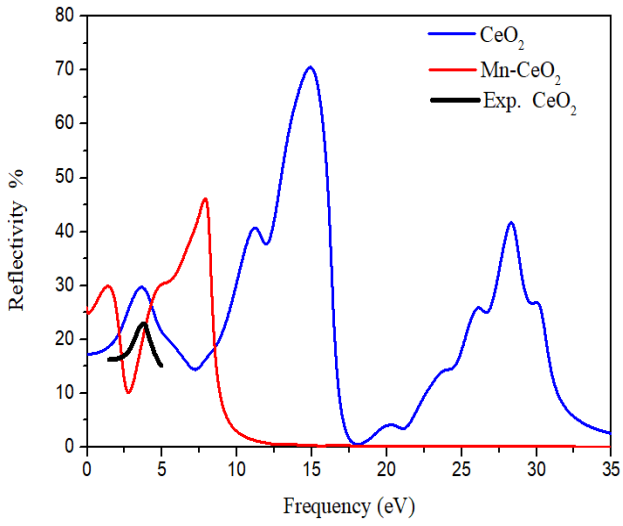


Fig. 12: Reflectivity. Experimental data of $CeO_2$ from reference [28].

## IV. CONCLUSIONS

A study was conducted on the atomic, electronic, and optical characteristics of $Ce_{1-x}Mn_xO_2$ ( x=0, 0.25) utilizing the DFT + U technique inside the GGA in the CASTEP software. The optical characteristics, bulk modulus, cell volume, and equilibrium lattice parameter computed for $CeO_2$ correspond quite well with experimental and other computed values. Ce-O bond length, bulk modulus, cell volume, and lattice parameter are all reduced when Mn is substituted for Ce in $CeO_2$ as compared to pure ($CeO_2$). The stronger chemical bond (Ce-O) in $CeO_2$ compared to $Ce_{0.75}Mn_{0.25}O_2$ is reflected in this. Cubic CeO2 experiences a decrease in band-gap (Eg) due to Mn substitutional doping. Selective light absorption and spintronic applications are possible with the doped system, which differs from the pure $CeO_2$ in a sharp spin dependent band gap ranging from 3.0 eV to 3.44 eV.

## CONFLICT OF INTEREST

Authors declare that they have no conflict of interest.

## REFERENCES

[1] M. Zhang, S. Zhang, Z. Qi, M. Xie, and Y. Qu, " Recent advancements in $CeO_2$-enabled liquid acid/base catalysis," *Catalysis Science and Technology*, vol. 14, pp. 225-240, 2024.

[2]D. F. Hammadi, R. S. A. Adnan, and M. A. Alsaraaf, "The Effect of $CeO_2$ Addition on Transformation Temperature and Wear Resistance of Cu-Al-Ni Shape Memory Alloy," *Engineering and Technology Journal*, vol. 40, No. 12, p. pp. 1712-1722, 2022.

[3]K. Chaibi, M. Benhaliliba and A. Ayeshamariam, "Computational Assessment And Experimental Study Of Optical And Thermoelectric Properties Of Rutile $SnO_2$ Semiconductor," *Superlattices And Microstructures*, vol. 155, 106923, 2021.

[4]M. Veszelei, L. Kullman, C. G. Granqvist, N. V. Rottkay and M. Rubin, "Optical Constants of Sputter-deposited Ti-Ce Oxide and Zr-Ce Oxide Films," *Applied Optics*, vol. 37, Issue 25, pp. 5993-6001, 1998.

[5] M. Miyauchi, A. Nakajima, T. Watanabe and K. Hashimoto, "Photocatalysis and Photoinduced Hydrophilicity of Various Metal Oxide Thin Films," *Chemistry of Materials*, vol. 14, Issue 6, pp. 2812-2816, 2002.

[6] F. Goubin, X. Rocquefelte, M. Whangbo, Y. Montardi, R. Brec and S. Jobic, "Experimental and Theoretical Characterization of The Optical Properties of $CeO_2$, $SrCeO_3$ and $Sr_2CeO_4$ Containing $Ce^{+4}$ ($f^0$) Ions," *Chemistry of Materials*, vol. 16, Issue 4, pp. 662-669, 2004.

[7] M. S. Park, S. K. Kwon, and B. I. Min, "Electronic Structure of Doped Anatase $TiO_2$: $Ti_{1-x}M_xO_2$ (M=Co, Mn, Fe, Ni)," *Physical Review B*, 161201, pp. 662-669, 2002.

[8] J. Anghel, A. Thurber, D. A. Tenne, C. B. Hanna and A. Punnoose, "Correlation Between Saturation Magnetization, Band Gap and Lattice Volume of Transition Metal (M=Co, Mn, Fe, Co or Ni) Doped $Zn_{1-x}M_xO$ Nanoparticles," *Journal of Applied Physics*, vol. 107, Issue 9, 09E314, 2010.

[9] J. J. Kim, S. R. Bishop, N. J. Thompson, D. Chen and H. L. Tuller, "Investigation of Nonstoichiometry In Oxide Thin Films By Simultaneous In Situ Optical Absorption And Chemical Capacitance Measurements: Pr-Doped Ceria, A Case Study," *Chemistry of Materials*, vol. 26, Issue 3, pp. 1374-1379, 2014.

[10] K. Li, H. Wang, Y. Wei and D. Yan, "Syngas Production From Methane And Air Via A Redox Process Using Ce-Fe Mixed Oxides As Oxygen Carriers," *Applied Catalysis B: Environmental*, vol. 97, Issue 3-4, pp. 361-372, 2010.

[11] K. S. Ranjith, P. Saravanan, S. H. Chen, C. L. Dong, C. L. Chen, S. Y. Che et al., "Enhanced Room-Temperature Ferromagnetism on Co-Doped $CeO_2$ Nanoparticles: Mechanism and Electronic and Optical Properties," *The Journal of Physical Chemistry C*, vol. 118, Issue 46, pp. 27039-27047, 2014.

[12] S. Kumar, Y. J. Kim, B. H. Koo, and C. G. Lee, "Structural and Magnetic Properties of Ni Doped $CeO_2$ Nanoparticles," *Journal Of Nanoscience And Nanotechnology*, vol. 10, pp. 7204-7207, 2014.

[13] D. Tian, C. Zeng, Y. Fu, H. Wang, H. Luo, C. Xiang, K. Li, and X. Zhu, "A DFT Study Of Structural, Electronic And Optical Properties Of Transition Metal Doped Fluorite Oxide: $Ce_{0.75}M_{0.25}O_2$ (M=Fe, Co, Ni)," Solid State Communications, vol. 231-232, pp. 68-79, 2016.

[14] M. Sharma, R. Adalati, R. Rani, S. Sharma, A. Kumar, N. Choudhary and R. Chandra, " Mn Incorporated $CeO_2$ Lattice Endorsement Of Electrochemical Performance In Symmetric Supercapacitor Devices," Energy Technology, vol. 11, Issue 10, 2300321, 2023.

[15] Y. Tang, H. Zhang, L. Cui, C. Ouyang, S. Shi, W. Tang, H. Li, J. Lee and L. Chen, "First-Principles Investigation On Redox Properties Of M-doped CeO2 (M=Mn,Pr,Sn,Zr)," Physical Review B, vol. 82, 125104, 2010.

[16]D. D. M. Prabaharan, K. Sadaiyandi, M. Mahendran, and S. Sagadevan, "Investigating The Effect Of Mn-Doped $CeO_2$ Nanoparticles By Co-precipitation Method," Applied Physics A, vol. 124, Issue 86, pp. 1-7, 2018.

[17] D. G. Pintos, A. Juan and B. Irigoyen, "Mn-Doped $Ce_2$: DFT+U Study Of Catalyst For Oxidation Reactions," The Journal Of Physical Chemistry C, vol. 117, pp. 18036-18073, 2013.

[18] A. M. Ali, "Hubbard Model Calculations For Zinc Oxide Semiconductor," University Of Thi-Qar Journal Of Science, vol. 10, No. 1, pp. 101-106, 2023.

[19] J. P. Perdew, A. Ruzsinszky, G. I. Csonka, O. A. Vydrov, G. E. Scuseria, L. A Constantin, X. Zhou and K. Burke, "Restoring The Density-Gradient Expansion For Exchange In Solids And Surfaces," *Physical Review Letters*, vol. 100, 136406, 2008.

[20] T. El-achari, F. Goumrhar, L. B. Drissi, and R. Ahl Laamara, "Structural, electronic andmagnetic properties of Mn doped $CeO_2$: An ab-initio study," *Physica B: Physics of Condensed Matter*, vol. 601, 412443, 2021.

[21] N. V. Skorodomova, R. Ahuja, S. I. Simak, B. Johansson and B. I. Lundqvist, "Electronic, Bonding And Optical Properties Of $CeO_2$ and $CeO_3$ From First Principles," *Physical Review B*, vol. 64, 115108, 2001.

[22]M. Michalska, K. Lemanski and A. Sikora, "Spectroscopic and structural properties of $CeO_2$ nanocrystals doped with $La^{3+}$, $Nd^{3+}$ and modified on their surface with Ag nanoparticles," *Heliyon*, vol. 7, e06958, 2021.

[23] H. Huang, J. Liu, P. Sun, S. Ye and B. Liu, "," *The Royal Society Of Chemistry Advances*, vol. 7, 7406, 2017.

[24] V. V. Hung, and L. T. M. Thanh, "Study of Elastic Properties of CeO2 By Statistical Moment Method," *Physica B*, vol. 406, pp. 4014-4018, 2011.

[25] H. Huang, J. Liu, P. Sun, S. Ye and B. Liu, "Effects Of Mn-Doped Ceria Oxygen Storage Material On Oxidation Activity Of Diesel Soot," *The Royal Society Of Chemistry Advances*, vol. 7, 7406, 2017.

[26] Y. Zhang, and X. Zhao, " Density Functional Study On Electronic And Optical Properties Of C (Or N)-Doped Cubic Cerium Dioxide," *Journal Of Solid States Chemistry*, vol. 182, pp. 3207-2310, 2009.

[27] P. Patsalas, S. Logothetidis, L. Sygellou, and S. Kennou, "Structure-dependent electronic properties of nanocrystalline cerium oxide films," *Physical Review B*, vol. 68, 035104, 2003.

[28] F. Marabelli, and P. Wachter, "Covalent insulator $CeO_2$: Optical reflectivity measurments," *Physical Review B*, vol. 36, No.2, 1987.